Monthly Notices
of the
ROYAL ASTRONOMICAL SOCIETY

Mon. Not. R. Astron. Soc. **406,** 2473–2487 (2010) doi:10.1111/j.1365-2966.2010.16772.x

Evidence for supernova-synthesized dust from the rising afterglow of GRB 071025 at $z \sim 5$

Daniel A. Perley,[1⋆] J. S. Bloom,[1] C. R. Klein,[1] S. Covino,[2] T. Minezaki,[3] P. Woźniak,[4] W. T. Vestrand,[4] G. G. Williams,[5] P. Milne,[5] N. R. Butler,[1] A. C. Updike,[6] T. Krühler,[7,8] P. Afonso,[7] A. Antonelli,[9] L. Cowie,[10] P. Ferrero,[11] J. Greiner,[7] D. H. Hartmann,[6] Y. Kakazu,[12] A. Küpcü Yoldaş,[13] A. N. Morgan,[1] P. A. Price,[10] J. X. Prochaska[14] and Y. Yoshii[3]

[1]*Department of Astronomy, University of California, Berkeley, CA 94720-3411, USA*
[2]*INAF/Osservatorio Astronomico di Brera, via Bianchi 46, 23807 Merate, LC, Italy*
[3]*Institute of Astronomy, School of Science, University of Tokyo, Mitaka, Tokyo 181-0015, Japan*
[4]*Los Alamos National Laboratory, Los Alamos, NM 87545, USA*
[5]*Steward Observatory, University of Arizona, 933 North Cherry Avenue, Tucson, AZ 85721, USA*
[6]*Department of Physics and Astronomy, Clemson University, Clemson, SC 29634-0978, USA*
[7]*Max-Planck-Institut für extraterrestrische Physik, Giessenbachstraße, D-85748 Garching, Germany*
[8]*Universe Cluster, Technische Universität München, Boltzmannstraße 2, D-85748 Garching, Germany*
[9]*INAF/Rome Astronomical Observatory, Via Frascati 33, 00044 Monte Porzio (Roma), Italy*
[10]*Institute for Astronomy, 2680 Woodlawn Drive, Honolulu, HI 96822-1839, USA*
[11]*Instituto de Astrofísica de Canarias, Vía Láctea s/n, 38200 La Laguna, Tenerife, Spain*
[12]*Institut d'Astrophysique de Paris, 98bis, Bd Arago, F-75014 Paris, France*
[13]*European Southern Observatory, Karl-Schwarzschild-str. 2, 85748 Garching, Germany*
[14]*UCO/Lick Observatory, Department of Astronomy and Astrophysics, University of California, 1156 High Street, Santa Cruz, CA 95064, USA*

Accepted 2010 March 31. Received 2010 March 31; in original form 2009 December 15

ABSTRACT

We present observations and analysis of the broad-band afterglow of *Swift* GRB 071025. Using optical and infrared (*RIYJHK*) photometry, we derive a photometric redshift of $4.4 < z < 5.2$; at this redshift our simultaneous multicolour observations begin at ∼30 s after the gamma-ray burst trigger in the host frame, during the initial rising phase of the afterglow. We associate the light-curve peak at ∼580 s in the observer frame with the formation of the forward shock, giving an estimate of the initial Lorentz factor $\Gamma_0 \sim 200$. The red spectral energy distribution (even in regions not affected by the Lyman α break) provides secure evidence of a large dust column. However, the inferred extinction curve shows a prominent flat component between 2000 and 3000 Å in the rest frame, inconsistent with any locally observed template but well fitted by models of dust formed by supernovae. Time-dependent fits to the extinction profile reveal no evidence of dust destruction and limit the decrease in the extinction column to $\Delta A_{3000} < 0.54$ mag after $t = 50$ s in the rest frame. Together with studies of high-z quasars, our observations suggest a transition in dust properties in the early Universe, possibly associated with a transition between supernova-dominated and asymptotic giant branch-dominated modes of dust production.

Key words: dust, extinction – gamma-ray burst: general – gamma-ray burst: individual: 071025.

1 INTRODUCTION

Starting with the discovery of the ninth magnitude afterglow of gamma-ray burst (GRB) 990123 (Akerlof et al. 1999), the early-time study of GRB afterglows has presented great promise to elucidate the nature both of the GRB phenomenon itself and of the medium surrounding these objects in extremely distant galaxies. Fast-responding telescopes, slewing to the burst location in time to catch the afterglow at or near the time of peak luminosity, can probe the physics of the explosion in the initial seconds as the ultrarelativistic outflow is decelerated by the interstellar medium

⋆E-mail: dperley@astro.berkeley.edu

(ISM). Continued observations can then follow the evolution of the reverse and forward shocks for many hours as the afterglow fades away, providing constraints on the still poorly understood early-time emission processes. In addition, the extreme luminosities at early times (e.g. Kann, Masetti & Klose 2007a; Racusin et al. 2008; Bloom et al. 2009) enable even very small telescopes to provide precise photometric and occasionally spectroscopic measurements of the afterglow spectral energy distribution (SED) and act as a probe of interstellar gas and dust out to the epoch of reionization (Kawai et al. 2006; Totani et al. 2006; Gallerani et al. 2008; McQuinn et al. 2008; Salvaterra et al. 2009; Tanvir et al. 2009; Greiner et al. 2009a). And while the usage of early-time SEDs as probes of the interstellar environment is hindered to some extent by the uncertain emission processes acting at these times, they nevertheless can provide constraints on the direct influence of a GRB on its surrounding medium in the form of dust destruction and photoionization (Waxman & Draine 2000; Fruchter, Krolik & Rhoads 2001; Draine & Hao 2002; Perna & Lazzati 2002; Perna, Lazzati & Fiore 2003).

At the same time, however, the fleeting and time-variable nature of GRB afterglows poses several challenges for these early-time diagnostics. To maximize sensitivity, the smallest telescopes typically do not employ filter systems and therefore give minimal frequency-domain information. When filters are employed, ordinary telescopes are forced to employ a filter cycle, creating the possibility of confusion between the spectral and temporal evolution of the event. Nevertheless, progress has advanced steadily with the commissioning of several simultaneous-colour robotic telescopes. The Peters Automatic Infrared Imaging Telescope (PAIRITEL; Bloom et al. 2006), online since late 2004, provides simultaneous measurements in the J, H and K_s bands every 7.8 s starting within 1–3 min of a typical GRB and is the primary subject of this paper. Notable PAIRITEL-followed bursts include GRBs 041219A, 061126 and 080319B (Blake et al. 2005; Perley et al. 2008a; Bloom et al. 2009). More recently, the seven-channel Gamma-Ray Burst Optical/Near-Infrared Detector (GROND; Greiner et al. 2008) has also produced simultaneous SEDs of afterglows at over the wavelength range of 4000–24 000 Å, including in several cases time-dependent SEDs during the afterglow rise and fall (Krühler et al. 2008, 2009b) and short-time-scale flares (Krühler et al. 2009a; Greiner et al. 2009b), and Rapid Telescopes for Optical Response-T (RAPTOR-T) has tracked spectral changes during the fading of GRB 080319B in several optical bands simultaneously (Woźniak et al. 2009). In all cases, colour evolution appears to be absent or modest, consistent with the lack of strong colour evolution in the generally less constraining measurements by filter-cycling instruments such as the *Swift* UltraViolet-Optical Telescope (UVOT; Oates et al. 2009). Correlation with the gamma-ray prompt emission and with X-ray flares (also thought to be associated with the prompt phase; Chincarini et al. 2007; Kocevski, Butler & Bloom 2007) is rare (Yost et al. 2007), but has been observed in some cases (Vestrand et al. 2005, 2006; Page et al. 2007; Racusin et al. 2008; Klotz et al. 2009; Krühler et al. 2009a). These multiband observations are particularly important for distinguishing the predictions of different models for the large variety of light-curve behaviour observed at early times: reverse shock (Sari & Piran 1999a), energy reinjection (Rees & Meszaros 1998), prompt emission (e.g. Kumar & Panaitescu 2000, 2008), outflow deceleration (Sari & Piran 1999b; Mészáros 2006), spectral breaks moving through the optical bandpass (Sari, Piran & Narayan 1998) and many others.

GRB 071025, detected by the *Swift* mission (Gehrels et al. 2004), provides among the best probes of the early-time behaviour of a GRB to date. While no secure spectroscopic redshift was attained [$z \sim 5.2$ was estimated from a low-quality High Resolution Echelle Spectrometer (HIRES) optical spectrum at Keck; Fynbo et al. 2009], the photometric SED presented here shows clear evidence of a Lyman α break in the observer-frame R band and indicates a photometric redshift of $4.4 < z < 5.2$ (Section 3.2), making this among the highest redshift bursts to date and one of only a few observed in simultaneous colours during prompt emission. Our infrared (IR) and optical observations start at ∼30 s after the burst in the rest frame and follow the rise, peak and fall of an afterglow in simultaneous rest-frame optical colours. In this paper, we use this unique data set to test various models for the origin of the early emission and conclude that it is likely due to the deceleration of the burst outflow into a uniform-density ISM, allowing estimation of the Lorentz factor Γ (Section 4.1). The *IYJHK* SED demonstrates the existence of a significant dust column obscuring a star-forming region at $z > 4.4$ and provides evidence that the dust at this epoch had different properties from dust that prevails along sightlines in the more nearby Universe, in agreement with the study of a high-z quasi-stellar object (QSO) by Maiolino et al. (2004). We suggest that this difference is reflective of an absence of evolved asymptotic giant branch (AGB) stars in these earliest epochs and search for (and place stringent limits on) signs of destruction of this dust by radiation from the GRB (Section 4.2). Throughout the paper, we use the convention $F \propto t^{-\alpha}\nu^{-\beta}$ and assume cosmological parameters $h = 0.71, \Omega_\Lambda = 0.7, \Omega_M = 0.3$.

2 OBSERVATIONS

2.1 *Swift*

At 04:08:54 UT on 2007 October 25,[1] the Burst Alert Telescope (BAT; Barthelmy et al. 2005) on-board *Swift* detected GRB 071025 and performed a rapid slew to the GRB location, beginning observations with the X-Ray Telescope (XRT; Burrows et al. 2005) at 146 s after the trigger. The BAT light curve is broad and only slowly variable: the flux rises slowly during the first ∼80 s and peaks several times before beginning a steady decay at ∼130 s. The GRB remains detectable above the background until *Swift* was forced to slew away from the position due to an Earth constraint at 422 s after the initial trigger. Observations resumed at 3500 s and tracked the afterglow using the XRT with no further large gaps in temporal coverage for the next ∼3 d, after which it became too faint to be detected. Details of our high-energy reduction pipeline are described in detail by Butler et al. (2007) for the *Swift* BAT and by Butler & Kocevski (2007) for the *Swift* XRT.[2]

Swift's UVOT (Roming et al. 2005) observed the field starting at 155 s, but detected no significant afterglow signal in any of its seven filters (Pagani et al. 2007). The non-detection is consistent with our photometric redshift, as outlined in Section 3.2.

2.2 PAIRITEL observations

The robotic IR observatory PAIRITEL consists of the 1.3-m Peters Telescope at Mt. Hopkins, Arizona, formerly used for the

[1]This trigger time will be used as the reference time in the remainder of the paper.

[2]*Swift* bursts occurring after these publications, including GRB 071025, have been processed using the same methods; these results are available online at http://astro.berkeley.edu/∼nat/swift/

Two-Micron All-Sky Survey (2MASS; Skrutskie et al. 2006), re-outfitted with the southern 2MASS camera. PAIRITEL, like 2MASS, makes use of two dichroics to image in the J, H and K_s filters simultaneously.

PAIRITEL responded to the initial Gamma-ray burst Coordinate Network (GCN; Barthelmy et al. 1995) alert at 74.3 s and slewed immediately to the source. Observations began at 162 s and continued uninterrupted until 3812 s, when due to a problem with the observing queue PAIRITEL temporarily slewed to another location. Observations resumed at 9108 s and continued for another 2 h. Raw data files were processed using standard IR reduction methods via PAIRITEL Pipeline III and resampled using SWarp (Bertin et al. 2002) to create final 1.0 arcsec pixel^{-1} images for final photometry. PAIRITEL's standard observing cycle is to take three 7.8-s exposures in immediate succession at each dither position. While the early afterglow is detected in even the shortest 7.8-s frames, the signal-to-noise ratio (S/N) was too low for reliable photometry, so the shortest exposures reported here consist of 23.4-s 'triplestacks', the sum of all three images at each dither position. These images were further binned at successively later times to further improve the S/N. The afterglow position, relative to 2MASS astrometric standards, is $\alpha = 355.0711583, \delta = +31.778575$ (J2000).

Photometry was performed in IRAF[3] using the PHOT task. Best results were achieved using aperture photometry with an aperture radius of 2.25 arcsec in the J band, 2.5 arcsec in the H band and 2.75 arcsec in the K_s band. Unfortunately, while conditions during the observations were generally clear, the night was not fully photometric, with variations in the transmission of up to 0.3 mag during the course of observations and additional significant fluctuations in the seeing. Calibration was therefore performed by re-determining the zero-point for each image individually by comparison to our secondary field standards (Section 2.1.1). Fortunately, the field of GRB 071025 is rich in bright field stars, and a total of eight nearby stars (present and well detected in even short exposures with reference uncertainties of <0.05 mag) were used to determine the zero-point. The statistical uncertainty on the zero-point (never more than 0.05 mag) is essentially negligible relative to other sources of error in all cases. Systematic sources of error are addressed in Section 3.4.

The large plate scale of PAIRITEL (2.0 arcsec pixel^{-1}) and the variable sub-pixel response function of the NICMOS3 arrays create a significant additional uncertainty in each position beyond ordinary photometric errors, estimated at $\sim$3 per cent by Blake et al. (2008). To quantify this uncertainty as accurately as possible, we constructed light curves for standard stars of different magnitudes in regions of the image free of defects by measuring the image-to-image magnitude variations of bright (source-dominated) stars. An additional uncertainty of $\sim$0.02 mag per position was required to incorporate the observed scatter in the photometry of these objects. Additionally, we examined fainter (sky-noise-dominated) stars to compare the IRAF-generated uncertainty to that observed in the zero-pointed light curve, finding the IRAF uncertainties to be too low by about 20 per cent in each filter. Therefore the final uncertainties on our photometry, reported in Table 1, were determined by increasing the IRAF uncertainty by 20 per cent and adding the result in quadrature with $0.02/\sqrt{N_{\rm pos}}$ mag, where $N_{\rm pos}$ is the number of unique dither positions per stacked image.

2.3 Rapid-Eye Mount observations

GRB 071025 also triggered Rapid-Eye Mount (REM; Zerbi et al. 2001), a robotic (Covino et al. 2004) telescope located at the European Southern Observatory (ESO) Cerro La Silla observatory (Chile). The REM telescope has a Ritchey–Chretien configuration with a 60-cm $f/2.2$ primary and an overall $f/8$ focal ratio in a fast moving alt-azimuth mount providing two stable Nasmyth focal stations. At one of the two foci, the telescope simultaneously feeds, by means of a dichroic, two cameras: REMIR (Conconi et al. 2004) for the near-IR (NIR) and REM Optical Slitless Spectrograph (ROSS; Tosti et al. 2004) for the optical. Both cameras have a field of view (FOV) of 10×10 arcmin^2 and imaging capabilities with NIR (1 μm, J, H and K) and Johnson–Cousins VRI filters. Observations of the GRB 071025 field began at 144 s after the trigger, although this initial H-band exposure did not detect the afterglow. The optical camera was unfortunately not operational due to maintenance, so exposures were acquired only in 1 μm, J, H and K.

The raw frames were corrected for dark, bias and flat field following standard procedures. Although the burst was at low elevation at the trigger time, seeing conditions were good and photometry was performed using a 3.5-pixel (1.2-arcsec) aperture. Conditions were not photometric, and so the zero-point was determined for each image individually in JHK bands using a subset of 2MASS-based standards. The 1 μm band (often referred to as z in previous work, though this filter has almost no overlap with the traditional SDSS z band), after taking into account the transmission of the ROSS/REMIR dichroic, is close to the MKO Y band[4] and so we treated this filter as a Y measurement, using the interpolated magnitudes in Table 2 (see Section 2.1.1) and basing the calibration on four reference stars well detected in all images.

2.4 RAPTOR observations

The RAPTOR experiment (Vestrand et al. 2002), operated by Los Alamos National Laboratory, consists of a series of small telescopes at the Fenton Hill Observatory in New Mexico. RAPTOR-S is a fully autonomous robotic telescope with a 0.4-m aperture and typical operating focal ratio $f/5$. It is equipped with a 1000×1000 pixel CCD camera employing a back-illuminated Marconi CCD47-10 chip with 13-μm pixels.

RAPTOR-S responded automatically to the localization alert and was on target at 04:10:14.95 UT, 81.3 s after the trigger time (4.2 s after receiving the GRB position). The rapid response sequence of RAPTOR-S consists of nine 5-s images followed by 20 10-s images and finally 170 30-s images for a total of $\sim$2 h of coverage (including 5-s intervals between exposures used primarily for readout). In order to improve the S/N, photometry was performed on co-added images. Aperture photometry was performed using the SExtractor package (Bertin et al. 2002), and the magnitude offsets between epochs were derived using several dozen field stars.

Because of the extreme redness of this afterglow, the unfiltered RAPTOR-S observations required a special calibration procedure. Although the effective wavelength of the response curve for RAPTOR-S is close to that of the standard R band, the SED of this

[3] IRAF is distributed by the National Optical Astronomy Observatory, which is operated by the Association of Universities for Research in Astronomy (AURA) under cooperative agreement with the National Science Foundation.

[4] http://www.ukidss.org/technical/instrument/filters.html; see also Hillenbrand et al. (2002).

Table 1. PAIRITEL observations of GRB 071025.

t_{start} (s)	t_{end} (s)	t_{exp} (s)	J (mag)	H (mag)	K_s (mag)
162.3	186.9	23.4	16.160 ± 0.452	15.933 ± 0.768	14.098 ± 0.413
197.6	222.1	23.4	15.448 ± 0.153	14.898 ± 0.198	13.751 ± 0.195
233.8	258.2	23.4	15.486 ± 0.160	14.589 ± 0.143	13.397 ± 0.138
269.9	294.4	23.4	15.300 ± 0.141	14.299 ± 0.103	13.259 ± 0.119
306.1	330.6	23.4	15.083 ± 0.143	14.072 ± 0.124	13.070 ± 0.131
342.4	366.9	23.4	14.814 ± 0.126	13.987 ± 0.112	12.905 ± 0.136
378.6	403.1	23.4	14.797 ± 0.117	13.956 ± 0.110	12.884 ± 0.110
414.8	439.3	23.4	15.058 ± 0.129	14.065 ± 0.117	12.854 ± 0.112
451.1	475.5	23.4	14.624 ± 0.091	13.817 ± 0.086	12.835 ± 0.098
487.2	511.6	23.4	14.669 ± 0.084	13.885 ± 0.082	12.606 ± 0.079
523.3	584.0	46.8	14.600 ± 0.064	13.774 ± 0.064	12.630 ± 0.064
595.7	656.4	46.8	14.801 ± 0.083	13.884 ± 0.071	12.919 ± 0.080
668.1	728.8	46.8	14.758 ± 0.073	13.913 ± 0.069	12.858 ± 0.073
740.5	801.2	46.8	14.677 ± 0.059	13.871 ± 0.057	13.007 ± 0.073
813.9	874.6	46.8	14.799 ± 0.088	13.977 ± 0.083	12.875 ± 0.095
886.3	946.9	46.8	14.942 ± 0.083	14.250 ± 0.083	13.136 ± 0.090
958.6	1019.4	46.8	14.982 ± 0.083	14.100 ± 0.076	13.111 ± 0.095
1031.1	1128.0	70.2	15.359 ± 0.099	14.466 ± 0.087	13.417 ± 0.094
1139.8	1236.7	70.2	15.374 ± 0.078	14.355 ± 0.061	13.355 ± 0.075
1249.4	1346.4	70.2	15.161 ± 0.080	14.384 ± 0.078	13.330 ± 0.090
1358.1	1456.0	70.2	15.247 ± 0.066	14.443 ± 0.063	13.311 ± 0.075
1467.7	1564.6	70.2	15.086 ± 0.052	14.257 ± 0.056	13.296 ± 0.068
1576.3	1673.0	70.2	15.064 ± 0.052	14.351 ± 0.061	13.465 ± 0.075
1684.7	1781.6	70.2	15.176 ± 0.052	14.405 ± 0.056	13.435 ± 0.073
1793.3	1890.2	70.2	15.193 ± 0.052	14.452 ± 0.054	13.528 ± 0.073
1901.9	1998.8	70.2	15.227 ± 0.054	14.527 ± 0.059	13.554 ± 0.082
2010.5	2107.3	70.2	15.302 ± 0.063	14.564 ± 0.066	13.525 ± 0.082
2120.1	2216.9	70.2	15.434 ± 0.066	14.573 ± 0.063	13.739 ± 0.094
2228.6	2325.6	70.2	15.543 ± 0.078	14.702 ± 0.066	13.775 ± 0.097
2337.2	2434.2	70.2	15.637 ± 0.066	14.763 ± 0.066	13.713 ± 0.087
2445.9	2542.8	70.2	15.644 ± 0.071	14.927 ± 0.078	13.887 ± 0.101
2555.5	2652.3	70.2	15.602 ± 0.082	14.959 ± 0.087	14.111 ± 0.125
2664.0	2760.9	70.2	15.848 ± 0.087	15.039 ± 0.087	14.006 ± 0.118
2772.6	2941.9	117.0	15.985 ± 0.094	15.100 ± 0.084	14.081 ± 0.116
2953.6	3196.4	163.8	16.004 ± 0.070	15.211 ± 0.072	14.078 ± 0.089
3208.1	3486.0	187.2	16.168 ± 0.075	15.455 ± 0.084	14.405 ± 0.111
3498.7	3812.9	210.6	16.314 ± 0.082	15.420 ± 0.075	14.415 ± 0.108
9108.8	12432.7	2152.8	17.680 ± 0.154	17.196 ± 0.226	16.074 ± 0.228
13132.0	16637.0	2269.8	18.344 ± 0.228	17.462 ± 0.245	16.564 ± 0.324

Note. Time values are measured from the *Swift* trigger (UT 2007 October 25 04:08:54). Magnitudes are in the 2MASS (Vega) system and not corrected for Galactic extinction.

Table 2. Optical–IR secondary standards.

α (deg)	δ (deg)	R (mag)	I (mag)	Y (mag)	J (mag)	H (mag)	K_s (mag)
355.016646	31.770287	17.046	16.379	16.095	15.678	15.203	15.069
355.025377	31.744127	13.699	12.469	11.816	11.297	10.683	10.476
355.034260	31.771452	18.039	16.210	15.318	14.824	14.211	13.949
355.037846	31.737404	14.231	13.684	13.418	13.095	12.717	12.627
355.049875	31.745661	15.978	15.439	15.211	14.942	14.622	14.563
355.058508	31.790998	13.740	13.229	12.990	12.734	12.426	12.385
355.058815	31.780569	16.792	16.262	16.043	15.775	15.457	15.385
355.066002	31.793428	–	15.960	15.668	15.310	14.894	14.839
355.068623	31.725666	17.911	16.674	17.607	16.794	16.042	15.371
355.077212	31.725382	14.820	14.314	14.042	13.832	13.567	13.506
355.105243	31.771235	15.358	14.765	14.452	14.137	13.762	13.709

Note. Magnitudes are observed values, not corrected for Galactic extinction, and are reported in the Vega system.

Table 3. Additional photometry of GRB 071025.

Telescope	$t_{\rm mid}$ (s)	Filter	$t_{\rm exp}$ (s)	Mag.	Flux (μJy)
RAPTOR	119.5	clear	45.0	>16.94	<608.9
Super-LOTIS	134.5	R	50.0	>19.46	<59.89
REM	470.0	Y	81.0	15.620 ± 0.240	1257.2 ± 249.3
Lick	2714.0	J	210.0	15.817 ± 0.030	792.9 ± 21.6
Magnum	10206.0	J	600.0	17.760 ± 0.059	132.4 ± 7.0
Kuiper	5098.5	I	1055.0	18.452 ± 0.085	113.6 ± 8.6
NTT	81101.0	J	5104.0	$20.780 \pm 0.270^{\rm x}$	$8.204 \pm 1.806^{\rm x}$
GROND	80505.0	g	–	>23.2	<2.44

Note. Only the first observation by each telescope is presented here as an example of the form and content of the complete table. The full table, containing all 80 data points, is available online (see Supporting Information).

burst (Section 3.2) indicates a sharp drop in the flux between I and R bands, likely due to the onset of the Lyman α forest. As a result, most photons detected by RAPTOR-S actually fall in the spectral region covered by the standard I filter.

Therefore, we tie the unfiltered data to I-band standards from the Lick calibration (Section 2.1.1). The offset $(m_{\rm C} - I)_{\rm star}$ between the unfiltered magnitudes and standard I was derived using seven well-measured stars in the vicinity of the GRB covering a narrow range of colours $0.5 < (R - I) < 0.66$. Assuming that the SED of the burst emission did not change significantly between the time of RAPTOR-S observations and the time when it was measured, we derived an approximate correction to $(m_{\rm C} - I)_{\rm star}$ to account for the extremely red colour of the GRB. We used a K5V model spectrum from Kurucz (1979) as a proxy SED matching the mean colour of our comparison stars. By folding both SEDs with response curves of RAPTOR-S and the standard I-band filter, we find $(m_{\rm C} - I)_{\rm GRB} = (m_{\rm C} - I)_{\rm star} + 0.74$ mag. The uncertainty of the derived zero-point is about 10 per cent; consistent with this, we measure a relatively small offset of -0.08 mag between the calibrated RAPTOR magnitudes and an extrapolation from later, filtered I-band observations using our light-curve model (see Section 3.1). Table 3 lists the final RAPTOR-S photometry.

2.5 Super-LOTIS observations

The Super-Livermore Optical Transient Imaging System (Super-LOTIS) is a robotic 0.6-m telescope dedicated to the search for optical counterparts of GRBs (Williams et al. 2004, 2008). The telescope is housed in a roll-off-roof facility at the Steward Observatory Kitt Peak site near Tucson, Arizona. Super-LOTIS triggered on GRB 071025 and began observations at 04:10:29 UT (95 s after the trigger), acquiring a series of R-band frames, which were reduced using standard methods. Unfortunately, because of the optical faintness of the afterglow and high sky background, the quality of the images is poor and even after extensive stacking the detection is marginal, particularly in the earliest few stacks. Photometry was performed using aperture photometry and our Lick R-band field calibration as detailed in Section 2.1.1.

2.6 Lick infrared observations

We acquired an additional series of IR observations using the 3-m Shane telescope at Lick Observatory equipped with the UCLA GEMINI IR camera (McLean et al. 1993, 1994). A total of nine exposures were acquired in J and K' bands simultaneously starting at 04:52:23 UT, integrating for 11 co-adds of 20 s each in J and 35 co-adds of 6 s each in K'. The IR afterglow was still very bright at this time and is clearly detected with an S/N $>$ 50 in individual exposures. Reduction was performed via direct subtraction of temporally adjacent exposures followed by division by a twilight flat. Photometry was performed using IRAF and an aperture of 2 pixels (1.4 arcsec); images were calibrated relative to the PAIRITEL magnitudes of five nearby bright field stars.

The response of the K' filter is significantly different from K_s and the GRB exhibits an apparent colour [$H - K \approx 1.0$ that is much redder than any field star used for comparisons (ranging between $H - K = 0.04$–0.18)]. To correct to K_s for direct comparison to the PAIRITEL data, we use an approximate correction of $K_s \approx K \approx K' - 0.07$ (Wainscoat & Cowie 1992), with this correction inferred from the reddest star in table 1 of that work (Oph S1, $H - K = 0.94, K' - K = 0.07^{+0.015}_{-0.025}$). The K to K_s colour term is assumed to be negligible. This is found to produce good agreement between Lick data and coeval PAIRITEL points. However, due to uncertain differences between the Lick, MKO and other filter sets and the intrinsic GRB spectrum itself the overall calibration offset could be as much as 0.05 mag, and as a result the Lick K photometry is not used in fitting.

2.7 MAGNUM observations

The Multicolour Active Galactic NUclei Monitoring (MAGNUM) 2.0-m telescope on Haleakala has been carrying out observations of active galactic nuclei and other variable objects (including GRBs) since 2001 (Yoshii 2002; Kobayashi et al. 2003; Yoshii, Kobayashi & Minezaki 2003). The telescope is equipped with dual optical and IR channels, allowing simultaneous observations in two bands.

We initiated MAGNUM observations starting at 06:59 UT, acquiring a sequence of dithered exposures over the next $\sim$2 h in a large number of filters, including *RI* in the optical channel and *YJHK* in the IR channel. The MAGNUM FOV is small, and generally only one star was present in the field and away from the chip edge at all dither positions. Therefore, only a single star was used to establish the calibration in each filter. In the H-, K- and Y-band observations, the star at $\alpha = 355.066002, \delta = 31.793428$ was used for this purpose; for R, I and J, the star at $\alpha = 355.058815, \delta = 31.780569$ was used. The second Y-band exposure unfortunately contained no usable reference star. However, comparison of exposures in other filters and at other points in the night suggests that conditions were photometric, and so calibration was achieved by comparison to the first Y-band exposure (with a small aperture correction.)

Table 4. PAIRITEL JHK_s secondary standards.

α (deg)	δ (deg)	J (mag)	σ	H (mag)	σ	K_s	σ
355.107649	31.795298	11.681	0.012	11.445	0.011	11.418	0.007
355.058508	31.790998	12.734	0.007	12.426	0.007	12.385	0.011
355.037846	31.737404	13.095	0.007	12.717	0.007	12.627	0.010
355.037722	31.708279	13.207	0.052	12.952	0.048	12.872	0.036
355.134554	31.744791	13.704	0.031	13.393	0.029	13.343	0.024
355.077212	31.725382	13.832	0.024	13.567	0.014	13.506	0.022
355.105243	31.771235	14.137	0.007	13.762	0.007	13.709	0.015

Note. Magnitudes are observed values, not corrected for Galactic extinction, and are reported in the 2MASS (Vega) system.

2.8 Kuiper observations

Shortly after the GRB trigger, we initiated imaging observations at the 1.54-m Kuiper telescope, operated by Steward Observatory and located on Mt. Bigelow. Observations began at 04:37:08 UT and continued until 08:55:41 UT, mostly in the *R* and *I* filters with some additional observations in *V*. Images were reduced and combined in IRAF using standard techniques. The *I*-band images were not dithered and so an archival fringe frame was used to subtract the fringe pattern. Photometry was performed in IRAF using secondary standards.

2.9 Late-time afterglow observations

To try to constrain the late-time ($t > 12$ h) behaviour of this burst, additional follow-up was carried out on the 3.6-m New Technology Telescope (NTT) and at GROND. We observed the burst location on NTT using the IR imager SOFI in a series of *J*-, *H*- and *K*-band exposures and additionally in the *H* band only on the following night. Photometry was calibrated relative to our IR secondary standards.

GROND is a seven-channel instrument which has been mounted on the ESO 2.2-m telescope at La Silla, Chile, since 2007 April. GROND began observations of GRB 071025 on 2007 October 26 at 01:50 UT and completed one 8-min observing block and two 20-min observing blocks. In total, nine images were taken in the g' r' i' z' bands and 216 were taken in the NIR. Each NIR image was 10 s long; the optical images varied in length from 137 to 408 s. The images were reduced using the GROND pipeline (Küpcü Yoldaş et al. 2008), with all images combined into a single stack for each filter. For consistency with other measurements, photometry was performed using aperture photometry calibrated to our secondary standards in *JHK*. For g' r' i' z' bands, images are calibrated directly relative to spectroscopic standard stars SA 114-750 and SA 114-656.

Poor agreement is observed between the NTT and GROND observations (and between the overall SED at this time and earlier data) using a standard 1-arcsec aperture, even though these epochs are effectively coeval. We have re-examined these data and find no clear evidence of problems in the reduction or photometry, although the afterglow appears extended in the north–south direction in the GROND *H*-band frame, suggesting that it might be blended with a nearby source or image artefact. No neighbouring source is observed in the NTT imaging, and the deep Keck optical imaging shows no object within ∼3 arcsec of the afterglow position (Section 2.1.0). However, to guard against this possibility we performed the photometry in the GROND *J* and *H* channels and all NTT channels using a small aperture (0.5 arcsec) in all bands. This smaller aperture provides good consistency between the two observations and is used in our analysis.

2.10 Keck observations

To help rule out a low-redshift origin for this burst, we imaged the field around GRB 071025 with the Low Resolution Imaging Spectrometer (LRIS; Oke et al. 1995) on the Keck I telescope on 2008 August 2 using the *g* and *R* filters simultaneously under excellent conditions. Total exposure times were 1050 s in the *R* band and 1140 s in the *g* band. Consistent with the large photometric redshift inferred from the SED, no significant flux due to a host galaxy was detected at the location of the optical/IR afterglow (the nearest object is a pair of faint point-like sources located 3 arcsec to the north-east). Forced photometry at the position of the optical afterglow, calibrated using unsaturated secondary standards, gives a limit (3σ) of $R > 26.5$ mag, $g > 27.0$ mag.

2.11 Field calibrations

To improve upon the photometric accuracy of 2MASS, we stacked together all observations of the GRB field acquired by PAIRITEL during the night of 2007 October 25 UT and calibrated a set of isolated, high-S/N stars present in the field in all or nearly all dither positions relative to 2MASS. These magnitudes were used in place of 2MASS magnitudes directly and are presented in Table 4.

For the optical filters, on the night of 2009 June 19 we observed the field of GRB 071025 using the Nickel 1-m telescope at Lick observatory. Conditions were photometric throughout the night. Three exposures were acquired in the *R* band and one each in *I* and *g* bands, and stars within the field were calibrated by comparison to repeated observations of PG 1633 and PG 2336 (Landolt 1992) at varying airmass, calibrating reference stars within the field. A second calibration was conducted on 2009 September 28 using repeated observations of standard fields PG 1633, PG 2336, PG 0213 and SA 110; the results were found to be completely consistent with the June calibration.

No field calibration was performed in the *Y* band. To calibrate the observations in this filter, we derived our own transformation equation for calculating *Y* magnitudes of reference stars given photometry in nearby bands by fitting a simple linear regression model to the photometry available online at the United Kingdom Infrared Telescope (UKIRT) webpage.[5] (The $Y - J$ colour was fitted as a linear function of $J - H$ and the residuals were then fitted to a linear function of $I - J$.) The transformation equation $Y = J + 1.104(J - H) - 0.11(I - J) - 0.03$ was found to accurately describe the observed *Y*-band magnitudes for the available standards (with photometry in all four bands) with an rms of <0.03 mag. We

[5] http://www.jach.hawaii.edu/UKIRT/astronomy/calib/phot_cal/fs_izyjhklm.dat

therefore applied this equation to calculate the Y magnitudes for secondary standards in the GRB 071025 field using the calibrated *IJH* photometry.

The final calibrated magnitudes for these stars are presented in Table 2.

3 ANALYSIS

3.1 Early-time afterglow evolution: rise, fall and reddening

All photometric observations of GRB 071025 during the first night are presented in Fig. 1. Several features are immediately apparent. First, the afterglow was caught during what appears to be its initial optical rise, brightening by ∼1.5 mag from the first detections to the peak in all filters. Secondly, the evolution is not single-peaked: a limited rebrightening is observed at ∼1800 s. Thirdly, the burst is extremely red, with $R - K \sim 6.5$ mag. Finally, no dramatic colour change is evident. This is not to say that there is no finer scale colour evolution; as will be discussed later, the best-fitting curves plotted in Fig. 1 correspond to a chromatic model which is shown to produce a large improvement in χ^2 relative to the monochromatic case.

The empirical model used to fit this burst is described in previous work (Perley et al. 2008b; Bloom et al. 2009). In brief, our method fits all data in all filters simultaneously using a series of summed Beuermann et al. (1999) broken power-law functions, in this case two per filter. The sharpness parameter s was fixed at 1 (allowing it to vary resulted in insignificant improvement to χ^2). For each component, the pre-break (rising) power-law index α_r is constrained to be the same for all filters, as is the post-break (fading) index α_f. The overall flux-normalization factor in each filter is arbitrary, determined by the best fit to the data. Colour change is modelled by assuming that any overall change takes the form of a variation in the intrinsic spectral index β, i.e. $F_{\nu,2} = F_{\nu,1} \times (\frac{\nu_2}{\nu_1})^{\Delta\beta 12}$. Colour is allowed to vary between components (simply using the above equation to tie the normalized flux parameters of each component) and between rising and falling segments of an individual component (by allowing the break time of the Beuermann function to vary as a function of frequency, using the central frequency of each filter).

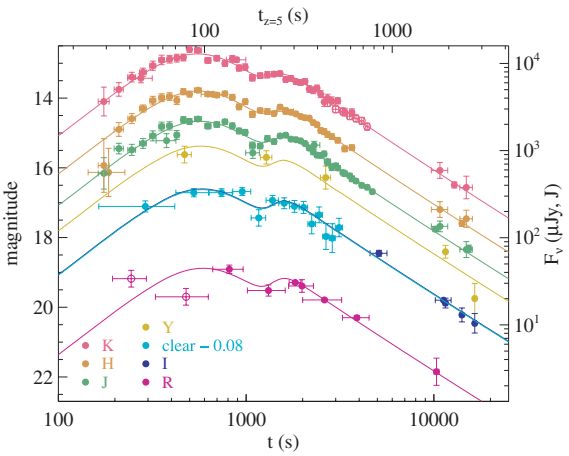

Figure 1. Early-time multiband optical and IR light curves of GRB 071025 fit to our empirical light-curve model. The afterglow is caught during its rise at ∼30 s in its rest frame (assuming $z = 5$) and exhibits a double-peaked structure before fading again as a simple power law. The RAPTOR unfiltered data have been shifted to match the I-band data. Magnitudes are Vega-based and not corrected for extinction.

Table 5. Light-curve best-fitting parameters.

Parameter	Symbol	Value
C1 rising index	$\alpha_{1,r}$	-1.66 ± 0.15
C1 fading index	$\alpha_{1,f}$	1.73 ± 0.21
C2 rising index	$\alpha_{2,r}$	-11.0 ± 2.1
C2 fading index	$\alpha_{2,f}$	1.27 ± 0.04
C1 peak time (s)	$t_{pk,1}$	575 ± 42
C2 peak time (s)	$t_{pk,2}$	1437 ± 17
Ratio of the C2/C1 peak flux	F_2	0.24 ± 0.03
Colour change across the C1 peak	$\Delta\beta_{1(rf)}$	-0.20 ± 0.14
Colour change between C1 and C2	$\Delta\beta_{12}$	-0.26 ± 0.12
Flux at $t = 10\,000$ s	F_R	5.76 ± 1.15
	F_I	34.4 ± 3.48
	F_Y	84.45 ± 8.66
	F_J	118.9 ± 4.79
	F_H	155.4 ± 6.26
	F_K	250.4 ± 15.1

Note. Summary of free parameters' fit in the light-curve model. Peak times are for the J-band filter. Flux parameters are not corrected for Galactic extinction; uncertainties include added systematics. 'C1' refers to the first light-curve component; 'C2' refers to the second component.

It should be emphasized that this method makes no assumptions about the overall SED, since only the *variation* in β is constrained. Indeed, the fitting method can be used to generate a best-fitting observed SED in all available filters, using all available data, at any chosen time (Section 3.2).

Two components (best-fitting parameters are summarized in Table 5) are found to provide an excellent fit to the data.[6] The light curve brightens quickly between our first detections at 180 s with a power law of approximately $\alpha_{1,r} = -1.66 \pm 0.15$ to a smooth peak at 580 s and then fades until about 1200 s. At that point the afterglow briefly re-brightens, peaking again at ∼1400 s before fading as a simple power law ($\alpha_{2,f} = 1.27 \pm 0.04$) for the remainder of our observations. The χ^2 residual, assuming no colour change, is 222.4 per 154 degrees of freedom (d.o.f.). Permitting colour change improves the fit significantly; allowing the parameters $\Delta\beta_{12}$ (describing the change in intrinsic spectral index between the first and second components after peak) and $\Delta\beta_{1(rf)}$ (describing the change in intrinsic index between rising and falling portions of the first component) to both vary, χ^2/d.o.f. improves to 197.4/152 which (according to the f-test) is significant at >99.9 per cent confidence. Most of this change is associated with the transition to the second component ($\Delta\beta_{12} = -0.26 \pm 0.12$ versus a non-significant colour change across the first peak of $\Delta\beta_{1(rf)} = -0.20 \pm 0.14$) but unfortunately, although the need for overall red-to-blue colour change is clear, its nature cannot be clearly distinguished by this methodology. We will further examine scenarios for this possible colour change in Section 4.2.

The X-ray light curve (Fig. 2) was fitted using a similar method (but with only a single 'filter', simplifying the process significantly). Again, two summed functions are found to provide an acceptable fit to the data. However, the first component is a rapidly declining, unbroken power law with $\alpha_{X,init} = 3.1 \pm 0.2$. This initial segment

[6]The first two Super-LOTIS points are an exception, both of which deviate from the fitted model by 2σ–3σ. Given the low S/N detections and a large degree of time binning in both cases, these points are not included in the fit, although the low flux observed in the second observational window, which covered the peak of the light curve, is nevertheless surprising given the behaviour in all three PAIRITEL bands and in RAPTOR data at that time.

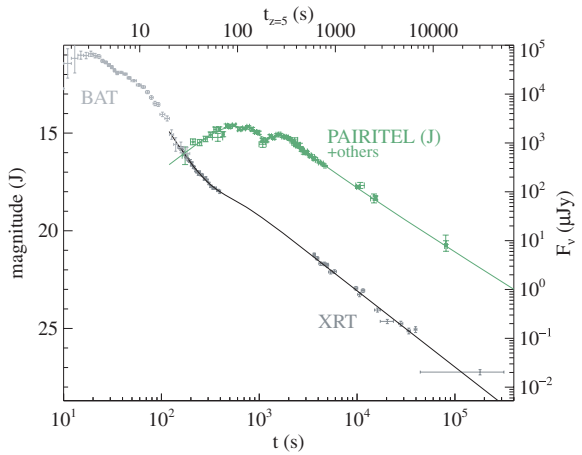

Figure 2. The gamma-ray (*Swift* BAT) and X-ray light curves (*Swift* XRT) of GRB 071025, compared to the *J*-band light curve out to late times. The X-ray light curve is rapidly fading during the optical–IR rise, probably due to high-latitude prompt emission (the light curve connects smoothly with the BAT light curve at these times if scaled to the X-ray flux, as shown.) Both optical and X-ray light curves fade with an unbroken decay at late times but with different decay slopes: $\alpha_{\rm opt} = 1.27 \pm 0.04$ versus $\alpha_{\rm X} = 1.56 \pm 0.03$.

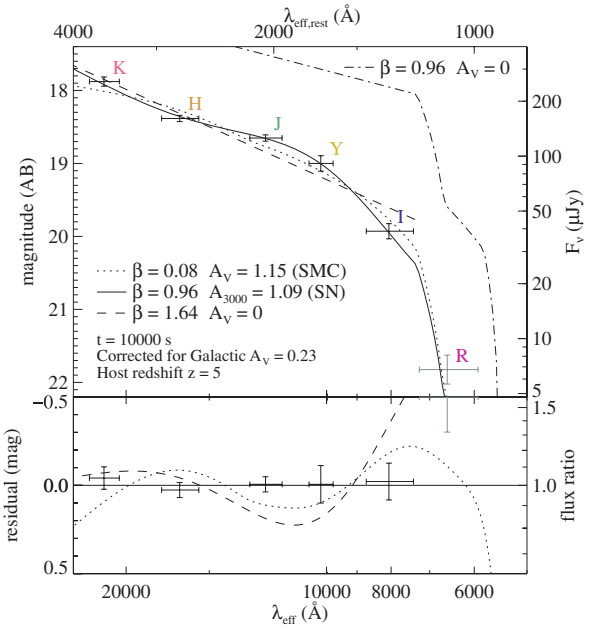

Figure 3. SED of GRB 071025 inferred from our broad-band photometry, fitted with different extinction models. Note the spectral flattening between *J* and *H* that contrasts with red $H - K$ and $I - Y$ colours. (The $R - I$ colour is due to absorption by the Lyman α forest.) Traditional models (such as SMC-like extinction, shown here as a dotted line) cannot reproduce this feature and give poor fit residuals (χ^2/d.o.f. = 20.8/2). The SN-dust model of Maiolino et al. (2004), shown as the solid line, is an excellent fit (χ^2/d.o.f. = 0.81/2). The dot–dashed line represents the intrinsic afterglow SED (for the SN model) without extinction applied but including our model of the IGM opacity at this redshift.

connects smoothly with the BAT prompt emission, as has been seen for a large majority of *Swift* bursts (O'Brien et al. 2006). The optical peaks unfortunately fall during an orbital gap in the XRT coverage, but by the end of the first observations the power law is already clearly flattening, almost certainly due to the transition from the rapid decay phase (O'Brien et al. 2006) to a standard afterglow (Nousek et al. 2006). Coverage resumes approximately an hour later, by which time the X-ray light curve is fading rapidly in an unbroken decay with $\alpha_{\rm X} = 1.56 \pm 0.03$.

3.2 SED and photometric redshift

At 10 000 s after the burst, the evolution of the light curve has given way to a simple power-law decay dominated by only a single component. Moreover, thanks to the MAGNUM observations, photometry is available in all colours within a relatively short timespan surrounding this epoch with a high S/N in *JHK*. We therefore choose this time as the extraction point for the overall SED of this burst, using the model fluxes from our fit as described above. (These fluxes are consistent with the MAGNUM and PAIRITEL photometry measured at this epoch specifically.) All fluxes are corrected for Galactic extinction (relatively small at $E_{B-V} = 0.07$ mag in this direction; Schlegel, Finkbeiner & Davis 1998).

The 1σ uncertainty on the fit parameter was combined in quadrature with an estimate of the calibration uncertainty in each filter. In the *J* and *H* filters, where the afterglow is comparable in colour to reference stars (which show a negligible scatter), we use an uncertainty of 0.04 mag; in *K* where the afterglow colour is much redder than our reference stars, we conservatively increase this to 0.06 mag. This incorporates both the absolute and relative calibration accuracy of 2MASS (estimated at ∼0.02 and 0.011 mag, respectively; Cohen, Wheaton & Megeath 2003 and 2MASS online documentation[7]), effects of variation of the effective wavelength $\lambda_{\rm eff}$ from its reference value due to a non-standard spectrum (<0.02 mag), the possibility of strong absorption from ISM or intergalactic medium (IGM) lines (very likely < 0.02 mag) and uncertainties in the extinction correction (< 0.01 mag). In the *Y* band, we use an estimate of the photometric scatter of the high-S/N REM reference stars to the interpolated secondary standards (0.1 mag). We also use 0.1 mag in the *I* band due to the redness of the afterglow in this band and the possibility that Lyman α may be affecting the flux towards the blue filter edge if the redshift is $z > 5.0$. In the *R* band a large uncertainty of 0.2 mag is used, although because *R* is almost certainly heavily blanketed by the Lyman α forest we use this filter only to place a limiting value on the redshift and exclude it from fits to the extinction profile. The resulting SED (fitted with various models, explained below) is plotted in Fig. 3.

The sharp drop-off towards the *R* band is suggestive of high redshift. However, the spectral slope observed even well redwards of this apparent break is quite red ($\beta \sim 1.64$, as shown by the dashed straight line in Fig. 3), suggesting that significant extinction is likely present as well. In order to quantitatively constrain the redshift *z*, we fit the data set with a large number of different extinction models (detailed in Section 3.3) at varying redshifts. Absorption due to the Lyman α forest is taken into account using a simple model of the average opacity of the IGM as a function of *z* and λ from Madau (1995). The extinction column A_V and the spectral index β were constrained to be positive: negative extinction is unphysical, while a negative spectral index would be both much bluer than any previously observed afterglow and in disagreement with standard afterglow theory (Sari et al. 1998).

The HIRES spectrum discussed in Fynbo et al. (2009) shows a trace extending from the limit of the spectral range at 7950 down to 7550 Å, bluewards of which no flux is detected. While the quality

[7]http://www.ipac.caltech.edu/2mass/releases/allsky/doc/sec4_8.html

of this spectrum is poor, the non-detection of Lyman α puts a robust upper limit on the redshift of $z < 5.2$, so this was treated as the maximum redshift. Regardless of the extinction law, no known dust curve is able to reproduce the extremely steep $I - R$ slope without invoking Lyman α blanketing of the R band, which becomes significant at $z \sim 4.0$. Even after including a variety of extinction templates (below), the lower limit on the redshift (95 per cent confidence) is $z > 4.4$. Treating redshift as a free parameter, the best-fitting z is dependent on the extinction law but is approximately $z = 4.8 \pm 0.2$ (1σ). In the remaining discussion, we will assume a fiducial value of $z = 5.0$; however, similar conclusions apply to other redshifts within the constrained range (4.4–5.2).

3.3 Extinction profile

Qualitatively, the SED presented in Fig. 3 is unusual among GRB afterglows due to the presence of an apparent inflection; while the $K - H$ and $Y - I$ colours are very red, between H and J bands the slope is quite flat. This flattening is quite significant (e.g. the H-band point is more than 0.2 mag below an interpolation between J and K) and suggests that the afterglow of GRB 071025 is subject to a complex reddening profile. To try to distinguish different possible models, we therefore fit many different extinction laws to the photometric SED, including Milky Way, Large Magellanic Cloud (LMC) and Small Magellanic Cloud (SMC) curves estimated using the parametrization of Fitzpatrick (1999) as implemented in the Goddard Space Flight Centre IDL astronomy user's library, the starburst-galaxy Calzetti curve (Calzetti et al. 2000) and the high-z QSO extinction law from Maiolino et al. (2004). The intrinsic spectral index β is free but limited to be $\beta > 0$. A summary of the goodness-of-fit χ^2 for each fit model is presented in Table 6.

A large family of models, including the Milky Way and LMC curves as well as the extinction curves derived from a few recent highly reddened GRBs (Krühler et al. 2008; Elíasdóttir et al. 2009; Prochaska et al. 2009) display a prominent 2175-Å bump. We can strongly rule out such a feature; at the observed redshift, the broad absorption signature would fall in or near the J band. Formal fits using these extinction templates (regardless of R_V) return A_V of zero in all cases (our fits do not permit negative extinction.)

An SMC-like extinction curve (dotted line in Fig. 3) provides a visually reasonable-looking fit to our data, but the χ^2/d.o.f. is unacceptable at 20.8/2. This is again no surprise: the SMC extinction curve increases rapidly and monotonically with a decreasing wavelength and cannot produce the flattening in our SED. The featureless Calzetti law similarly produces a poor fit because it cannot produce the deviations from a power law evident in the photometry.

We also attempted a general fit using the full parametrization of Fitzpatrick (1999), but even if the γ and x_0 parameters of this model are fixed and the c_1 and R_V parameters are tied to c_2 using, e.g., the correlations of Reichart (2001), the solution is underdetermined. If the intrinsic spectral slope β is fixed, the solution is exactly determined; for, e.g., $\beta = 0.65$, we derive $R_V = 5.26 \pm 0.53$, $c_2 = 0.17 \pm 0.12, c_3 < 0.2, c_4 = 1.03 \pm 0.32, \chi^2$/d.o.f. = 1.49/0. However, this combination of parameters (small c_2 and low or zero c_3, indicating a shallow near-UV extinction law and a negligible 2175 Å bump) is unlike any sightline in the local Universe observed to date. We also fit the data to the general extinction curve of Li et al. (2008b), fixing $\beta = 0.65$ and $c_4 = 0$ to avoid underdetermination, but the c_1 and c_3 parameters did not converge.

However, one previously observed extinction law performs extremely well at matching the observed features. Maiolino et al. (2004) presented observations of the reddened $z = 6.2$ broad absorption-line quasar SDSS J104845.05+463713, comparing NIR spectroscopy of the source to optical spectra of low-redshift quasars of the same class to estimate the extinction law. The inferred curve of this object is notable for a distinct flattening between 1800 and 3000 Å and was interpreted (and modelled quantitatively) by that paper as the signature of dust synthesized in supernova (SN) explosions. We fit a polynomial to the solid ($Z = 10^{-4}\,Z_\odot, M = 25\,M_\odot$) curve displayed in fig. 2 of that paper and used the resulting extinction curve to fit our observed photometry.[8] The result is an excellent match (χ^2/d.o.f. = 0.81/2) and is shown by the solid line in Fig. 3. The associated extinction column is $A_{3000} = 1.09 \pm 0.20$ mag.[9]

The best-fitting value of the intrinsic spectral index β_{IR} as inferred at the SED extraction epoch is $\beta_{IR} = 0.94 \pm 0.14$, quite typical of other afterglows at this stage. This value is also consistent (albeit only marginally) with the theoretically expected value based on the observed X-ray spectral index (intrinsic $\beta_X = 1.15 \pm 0.12$) if a cooling break is present between IR and X-ray bands (in this case, $\beta_{IR} = \beta_X - 0.5 = 0.65 \pm 0.12$). Imposing this constraint as a prior on the fit to A_{3000} and β_{IR}, we measure $A_{3000} = 1.27 \pm 0.20$ mag.

Alternatively, the SED is also consistent with the absence of a cooling break; at the extraction epoch the combined IR-through-X-ray SED is well fitted (χ^2/d.o.f. = 1.14/3) by a single power law with $\beta_{IR,X} = 0.88$ and $A_{3000} = 1.19 \pm 0.20$ of the Maiolino dust, both consistent with the values inferred from the optical data alone. However, the X-ray flux at this time is clearly fading faster than the optical light curve (Fig. 1); if this is not due to the presence of a moving spectral break such as a cooling break, the spectral index itself would have to be slowly evolving (implying evolution in the electron index p).

In support of our general conclusion of a significant amount of dust extinction, we note that a large amount of absorption is inferred from the X-ray spectrum also: we measure an equivalent column of $N_H = (3.2 \pm 0.8) \times 10^{22}$ cm^{-2}. Although the scatter in the ratio of A_V/N_H for *Swift* bursts is nearly an order of magnitude, using the average value from Schady et al. (2007) this column corresponds to an extinction of $A_V \sim 4$ mag.

Table 6. Results of extinction fits.

Dust model	β	A_V (mag)	R_V	χ^2/ d.o.f.
None	1.64 ± 0.08	0		33.3/3
SMC	0.08 ± 0.42	0.12 ± 20.6	2.73	20.8/2
MW	1.64 ± 0.08	<0.07	3.1	33.3/2
LMC	1.64 ± 0.08	<0.07	3.2	33.3/2
GRB 080607	1.64 ± 0.08	<0.12	4.0	33.3/2
Calzetti	0.00 ± 0.80	1.42 ± 0.68	4.0	25.3/2
Fitzpatrick	0.65	2.52 ± 0.97	5.26 ± 0.53	1.49/0
Maiolino SN	0.96 ± 0.14	1.09 ± 0.20^a		0.81/2

Note. Summary of key parameters from fits of various dust models to the SED of GRB 071025 as modelled at $t = 10\,000$ s. A redshift of $z = 5$ is assumed in all cases.
[a]Value is A_{3000}.

[8]Our K-band point is not covered by this figure, as the corresponding rest wavelength is shifted out of the IR window at $z = 6.2$. We assume an approximately linear extinction law in $1/\lambda$ below $\lambda_{rest} < 3300$ Å.
[9]The Maiolino extinction curve is normalized to A_{3000} instead of A_V (the V band at $z > 5$ is shifted into the mid-IR).

3.4 Further investigations of the IR calibration

The inference of SN-type dust for this object depends sensitively on the accuracy of our photometric calibration, and statements of its significance relative to the SMC fit depend equally critically on the precision in the *JHK* bands being as good as we claim; the Maiolino model is no longer preferred at >95 per cent confidence if, for example, an additional uncertainty of >0.075 mag (in addition to the systematic uncertainties already applied; Section 3.2) is added in quadrature to all SED data points or if >0.1 mag is added to just the *H*-band point (dependence on the other data points is much more robust: an addition of >0.2 mag to *K* is required and any one of the *J*, *Y* or *I* points could be removed completely). Therefore, we have scrutinized in detail our IR calibration procedures with particular emphasis on the PAIRITEL data. Because of the large number of exposures and a large number of calibration stars detected at a high S/N, the statistical errors on the zero-point are small. The possible sources of systematic uncertainty (beyond the minor effects we have already discussed and included) we have considered include the following.

Instrumental colour terms. PAIRITEL uses the same telescope, filter and camera system as the 2MASS survey, and so there is no reason to expect colour terms associated with the optics to be present. However, the presence of a significant bandpass difference could cause systematic discrepancies in calibration relative to field stars (see also Section 2.6), in particular in *H* and *K* bands where the afterglow colour is much redder than any of the bright stars used for calibration. We inspected the magnitudes derived from stars in our deep stack as compared to the stars in 2MASS to search for a correlation between the magnitude offset and colour; none was found.

Strong atmospheric variations in the effective filter bandpass. The IR absorption bands associated with water in Earth's atmosphere exhibit time variability, even within the observational windows. In particular, the exact shape of the *J*-band transmission function depends on the amount of precipitable water vapour (Cohen et al. 2003; however, the effect is small, with less than 2 per cent variation in relative magnitudes), and the *H* band contains a water ice absorption band which could introduce similar variations. Time-dependent absorption may therefore introduce temporary colour terms not evident in the all-night stack. Therefore, we carefully inspected the time evolution of the observed zero-points in all three bands. A small amount (up to 0.3 mag) of total transmission variability is indeed observed during the first 20 min, after which the zero-point in all three bands is nearly constant within uncertainties. No significant variation is observed in the difference between zero-points in different PAIRITEL bands nor is any correlation observed between the overall zero-point and the difference in zero-points between two bands that would suggest chromatic variations in the transmission. Furthermore, the zero-point appears constant (within our uncertainties) after ∼1400 s (the SED is determined at 10 000 s). The MMT Observatory cloud camera[10] shows no evidence of significant cloud cover at any point during the night, and weather archives indicate warm and stable conditions during the observation. Furthermore, in addition to PAIRITEL (Arizona), the Lick *J*-band (California) and MAGNUM (Hawaii) coeval measurements both give consistent results for the IR magnitudes, giving additional confidence in our results; in particular, both PAIRITEL and MAGNUM *JHK* data sets show the putative extinction feature independently. Therefore, we have no reason to believe that our SED is significantly affected by absorption features in Earth's atmosphere.

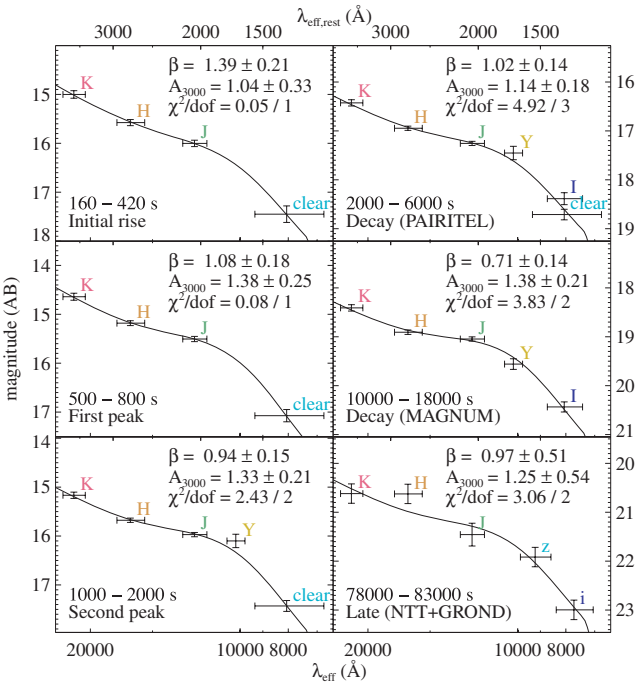

Figure 4. Time-dependent SED of GRB 071025 inferred after dividing the data into six different windows and re-fitting the flux parameters at each epoch using the light-curve model. The resulting SED is then fitted for spectral index β and extinction column A_{3000} at each epoch individually using a Maiolino extinction profile. The characteristic flattening between *J* and *H* bands is observed at every epoch (except at late times, when photometric errors are large) with no significant variation in its strength, increasing our confidence that it is a feature extrinsic to the GRB.

Intrinsic deviation of the GRB spectrum from a power law. We have assumed in our fits that the intrinsic spectrum of the GRB was a simple power law, as generally predicted by synchrotron theory. This assumption could, in principle, be violated. However, the most natural deviation from a power-law SED that might be expected (a spectral break within the optical/IR band) would create downward curvature in the intrinsic SED and actually require additional dust to produce the upward inflection feature that is observed. An SED modelled as the sum of two components (a steep power law dominating the *K* band and a shallower power law dominating the *J* band) would produce upward curvature, but cannot reproduce the sharpness of the observed feature unless the spectral index of the steep power law is unrealistically red ($\beta > 4$). Additionally, it would be surprising that both components would rise and fall in sync with each other throughout the complex early evolution of the light curve, as is observed. Indeed, evidence for the Maiolino-like dust is observed at every epoch with no significant variation in its strength or wavelength (Fig. 4; see also Section 4.2) with the exception of the final (GROND+NTT) SED, when the photometric uncertainties are too large to place any strong constraints on the extinction law.

Absorption from a damped Lyman α host system or Lyman α forest. If the host galaxy is at the maximum redshift of $z = 5.2$, our mean-opacity model of the Lyman α forest may significantly underestimate the impact of hydrogen absorption on the *I* band. To represent the most extreme possible case, we reran our dust models after adjusting the *I*-band flux upwards by 20 per cent (the

[10] http://skycam.mmto.arizona.edu/

approximate maximum diminution expected in the Kuiper *I*-band filter assuming 100 per cent opacity bluewards of 7550 Å, the limit on any DLA imposed by the HIRES spectrum) at $z = 5.2$. Even in this case, the Maiolino dust profile is strongly preferred (χ^2/d.o.f. = 2.5/2 versus 11.9/2 for SMC-like dust).

4 DISCUSSION

4.1 Rise of the forward shock and constraints on the Lorentz factor

The nearly achromatic first peak in the light curve shows the major hallmarks of the initial rise of the afterglow due to hydrodynamic deceleration of the fireball: a steep rise with no significant evidence of colour change across the peak. Alternative possibilities can be generally ruled out: for example, the transition of the synchrotron peak frequency (which would also produce a peak were it is to occur after the initial deceleration) would rise slowly and exhibit a blue-to-red colour shift of $\Delta\beta = (p - 1)/2 - (-1/3) = p/2 - 1/6$, completely incompatible with the observed absence of colour change or even limited red-to-blue evolution at this time. If the peak were due to dust destruction we would also expect significant colour change during the rise itself, which is not apparent in the data. (We will examine the possibility of dust destruction in more detail in Section 4.2.)

Within the category of hydrodynamical effects, there are then three possibilities for the rise of the afterglow: peak of the reverse shock, peak of the forward shock or an off-axis jet.

We will first consider the jet model (Granot et al. 2002; Granot 2005). In this case, the outflow is assumed to be strongly collimated with an observer located outside both the jet opening angle θ (observing angle $\theta_{\rm obs}$) and Lorentz cone $1/\Gamma$ (for a uniform jet; the theory can be suitably modified for a structured outflow: Kumar & Granot 2003). As the jet decelerates, a peak in the light curve will be observed once the flow has decelerated sufficiently for the $1/\Gamma$ cone to expand past the observer line of sight; this model has shown reasonable success representing the rising light curves of e.g. XRF 080330 (Guidorzi et al. 2009) and GRB 080710 (Krühler et al. 2009b). However, we are disinclined to favour this model on the grounds that it is expected to produce a very rapid post-break decay ($\alpha > 2$), which is not observed at late times ($\alpha_{2,\rm f} = 1.27 \pm 0.04$). This could be accounted for by associating the second component (which dominates the late-time decay) with an on-axis wide jet undergoing its initial rise (as in Krühler et al. 2009b), but this model is somewhat contrived in our case, requiring fine-tuning of the physical properties of the two jets to accommodate the large variation in their jetting times while still ensuring that they peak within a factor of $\sim$2 in time and flux. Alternatively, refreshed shocks and continuous energy injection out to late times could also be invoked to explain the two-peaked structure and lack of late decay within this model. Even in that case, another criticism of this model is that the isotropic energy release observed for this burst ($E_{\rm iso} = 6.5 \times 10^{53}$ erg) is not expected for a burst seen off-axis.

Next, we consider if the initial rise could be due to the reverse shock (Sari & Piran 1999a). This model is particularly attractive, as the overall light curve qualitatively looks impressively similar to the theoretical curve of Zhang, Kobayashi & Mészáros (2003): the first peak corresponds to the reverse shock and the second peak to the forward shock. However, the initial rise is somewhat slower than expected from simple analytic models. The assumed reverse shock rising index $\alpha_{1,r}$ depends on the assumed zero time t_0 (which was set to the trigger time in the above fits), but t_0 would need to be shifted back in time by an amount greatly in excess of the duration of the burst itself to match $t^{3p-5/2}$ predicted for the reverse shock rise in the slow-cooling case (Kobayashi 2000). The alternate fast-cooling case predicts a slower rise (too slow: $t^{13/16}$) and also a bluer spectrum than is preferred by our extinction modelling. A wind model also requires fast-cooling and a blue spectrum, and an even slower rise ($t^{1/2}$). Therefore a reverse shock is not our preferred paradigm either, though we are hesitant to rule it out on the basis that the known complexity of early afterglows and the failure of even late-time closure relations to properly predict the decay rate α (e.g. Rykoff et al. 2009) suggest that the quantitative details of light-curve behaviour may not be an especially reliable way to evaluate different models.

The most straightforward scenario for the initial rise is the formation of the forward shock as the burst ejecta decelerates into the surrounding medium (e.g. Rees & Meszaros 1992). In this case $\alpha = -2$ for $\nu < \nu_c$, which is still somewhat too fast but still consistent with the data within 2σ if t_0 is moved backwards in time by about 30 s. In this model, the second peak is presumably due to additional energy input from the central engine into the forward shock, perhaps in the form of a slow-moving shell that catches up at around 1 ks (Rees & Meszaros 1998). This model is generally consistent with all available observations including the apparent rapid rise of the second component, though the observed significant (albeit minor) colour change is not predicted. It could be due to the passage of a cooling break (though this would imply $\nu > \nu_c$ initially and a too-steep $\alpha = -3$ during the rise) or another effect such as variation in the electron index p.

Interpreting this feature as a forward shock enables us to measure the initial Lorentz factor of the explosion. Following e.g. Mészáros (2006) and Rykoff et al. (2009), this can be estimated from observable parameters via the following relationship:

$$\Gamma_0 = 2\Gamma_{\rm dec} = 2\left(\frac{3E_{\rm iso}}{32\pi n m_{\rm p} c^5 \eta t_{\rm pk,z}^3}\right)^{1/8} = 560\frac{3E_{\rm iso,52}}{\eta_{0.2} n_0 t_{\rm pk,z,10}^3}.$$

Here $E_{\rm iso,52}$ is the isotropic-equivalent energy release in units of 10^{52} erg, $\eta_{0.2}$ is the radiative efficiency in units of 0.2, n_0 is the circumburst density in units of cm^{-3} and $t_{\rm pk,z,10}$ is the afterglow peak time as observed at the burst redshift z in units of 10 s. For GRB 071025, using $E_{\rm iso} = 6.5 \times 10^{53}$ erg from our spectral model of the BAT data (at $z = 5$), we derive

$$\Gamma_0 \sim 206\eta_{0.2}^{-1/8} n^{-1/8}.$$

Compared to direct pair-opacity lower limits inferred by the *Fermi* Large Area Telescope (Abdo et al. 2009a,b), this is a relatively low value of Γ. However, it is fairly typical of afterglow-inferred values (100–1000; Molinari et al. 2007; Oates et al. 2009; Rykoff et al. 2009; Krühler et al. 2009a,b). This may indicate a difference in the types of populations probed by the two methods: the intrinsic delay in optical follow-up can measure Γ only for bursts for which the peak is quite late (low Γ) while high-energy photons themselves escape only if Γ is large. Hopefully, in the near future a joint *Swift–Fermi* burst with a luminous afterglow will allow both methods for estimation of the Lorentz factor to be compared.

4.2 Colour evolution: limits on dust destruction

Because of the need for $\nu_{\rm IR} < \nu_c$ to explain the slow rise, there is no explanation within the standard assumptions of afterglow theory

for the colour change observed during the afterglow. One possible solution would be to invoke a time-variable electron index p at early times; a softening of the electron distribution during the complex early evolution would cause a corresponding softening of the afterglow emission.

Another intriguing possibility, however, is the photodestruction of dust along the GRB line of sight (Waxman & Draine 2000; Draine & Hao 2002). While we have ruled out this model as being the predominant origin of the rise of the light curve based on the modest or absent colour change during the rising phase, it is still possible that it is occurring on a more subtle level. Because our light-curve model assumes that any colour change is associated with a temporal break, it is not clear that such a change would be manifest in those models. As a result, we have scrutinized the overall colour evolution of this GRB in significant additional detail to search for time evolution in the extinction column A_V.

The large flat (grey) component of the Maiolino SN-type extinction law has the useful feature that the observed spectral slope of an SED measured over this region will closely match the intrinsic spectral slope even for a large extinction column, breaking the degeneracy between the intrinsic spectral index β and amount of reddening A_{3000}. At $z \sim 5$, the $J - H$ colour (where the extinction law is grey) is affected only by the intrinsic spectral index and is nearly independent of A_{3000}, while $H - K$ and $J - I$ are affected by both the intrinsic index and reddening. This allows us to fit for β and A_{3000} independently with reasonable reliability, even with only a small number of points in the SED.

We have therefore undertaken time-variable extinction fits using simultaneous measurements by mosaicking the PAIRITEL *JHK* data to temporally match the early-time RAPTOR points, which are a good approximation of the I band (after a small adjustment of -0.08 mag; see Section 2.4 and Fig. 1). Dust models were fitted to this four-point SED as in Section 3.3. Results are plotted in Fig. 5.

As in the case of the complete data set, a Maiolino dust model is significantly preferred, with no evidence of evolution. In particular, the first mosaic (the only one contemporaneous with bright X-ray prompt emission, which is probably the dominant contributor to dust destruction; Fruchter et al. 2001) gives a modest value of $A_{3000} = 1.03 \pm 0.31$, fully consistent with our measurement at 10 000 s. The corresponding 95 per cent confidence limit on the decrease in the extinction column is $\Delta A_{3000} < 0.54$ mag. As we observe the H band ($\lambda_{\rm eff} \sim 2770$ Å in the host frame) rising by at least 1.5 mag between our first REM and PAIRITEL observations and the peak, this clearly rules out dust destruction as the cause of the early peak, consistent with our conclusions of the chromatic light-curve modelling in Section 4.1. The entirety of the colour variation appears to be due to variation in the intrinsic spectrum.

The significant dust column, combined with the lack of variability even during the end of the prompt phase, places a limit on the proximity of this dust to the GRB. The simulations of e.g. Perna et al. (2003) suggest that for a bright GRB virtually all dust within about 10 pc of the GRB will be destroyed, and significant destruction will be observed even out to 100 pc. While the exact constraints for this event will likely depend on detailed modelling of GRB 071025 specifically, this gives an approximate limit on the distance of the inferred absorbing dust column from the progenitor of at least $\gtrsim$10–100 pc.

5 CONCLUSIONS

GRB 071025 joins a growing list of GRBs caught early enough in their evolution to observe the rise and peak of the optical afterglow.

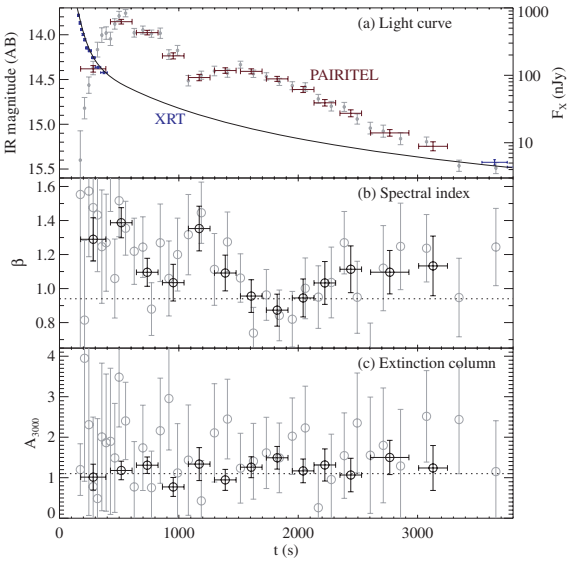

Figure 5. Models of colour evolution in the afterglow of GRB 071025. (a) IR and X-ray light curves of GRB 071025 from PAIRITEL and the *Swift* XRT showing the divergent behaviour in the two bands at these times. The early X-ray light curve is probably dominated by prompt emission, which is continuing in the BAT as well during this early decay phase. (b) The IR/optical spectral index β, as measured by a fit to PAIRITEL *JHK* and RAPTOR unfiltered data. Fixed extinction $A_{3000} = 1.1$ mag is assumed. The SED is observed to redden significantly during the observations. Grey points indicate fits to PAIRITEL *JHK* photometry only. (c) The time-dependent extinction column A_{3000} as measured by PAIRITEL and RAPTOR. The spectral index β is also free to vary in these fits. No evidence for variation in the extinction column is observed, ruling out dust destruction after ∼150 s.

Interpreting this as the initial rise of the forward shock, we estimate $\Gamma \sim 200$ for typical ISM densities. The mild red-to-blue colour evolution of the afterglow appears to be due to unknown intrinsic properties of the forward shock, rather than dust destruction due to irradiation of the burst environment. All of these properties are similar to those inferred from early-time observations of other GRB afterglows.

However, the extinction law we measure is nearly unique. Most afterglows with well-characterized SEDs show little extinction (Kann et al. 2007b), and events for which significant extinction has been observed have most commonly shown simple SMC-like profiles (e.g. Kann, Klose & Zeh 2006; Schady et al. 2007), characterized by significant curvature (strong wavelength dependence) but no spectral features. More rarely, featureless or even grey light curves with no significant curvature have been inferred for some bursts (e.g. Savaglio & Fall 2004; Stratta et al. 2005; Chen, Li & Wei 2006; Li, Li & Wei 2008a; Perley et al. 2008a), and recently a small number of events have been discovered containing the clear signature of the 2175-Å bump present in the Milky Way and LMC (Krühler et al. 2008; Elíasdóttir et al. 2009; Prochaska et al. 2009), though the details of these extinction curves show some differences from the average Milky Way ISM law. But to our knowledge, no other GRB sightline has shown clear evidence of dust not well fitted either by a local extinction template or by a simple, featureless law.

A possible exception is $z = 6.3$ GRB 050904. For this GRB, an analysis by Stratta et al. (2007) favoured the SN-type dust of Maiolino et al. (2004) over standard SMC, Milky Way and Calzetti models. Taken together, these two bursts would represent compelling evidence of an association between the observed dust model

and the chemical evolution of the Universe itself: to date, these events are the only bursts at $z \gtrsim 4.5$ showing evidence for significant extinction (all other bursts for which useful constraints on the extinction law have been possible are at $z \lesssim 4$; Kann et al. 2007b).[11]

Strong chemical evolution of the dusty ISM is to be expected at $z \sim 5$–6; while most dust at low-to-moderate redshifts is thought to have been produced in AGB stars, during the first ∼1 Gyr following the big bang there had not yet been time for these stars to form in large numbers (Morgan & Edmunds 2003). The cosmic age of 1.1–1.4 Gyr (assuming standard cosmological parameters with ΛCDM) allowed by our photometric redshift suggests that SN-like dust[12] is still the predominant source of obscuration in galaxies at this epoch and could provide important constraints on the evolution of the first galaxies and the production of early dust grains (e.g. Dwek, Galliano & Jones 2007; Valiante et al. 2009). We note that the extinction column inferred from this galaxy is even larger than that inferred from the $z = 6.2$ QSO ($A_{3000} = 0.4$–0.8 mag; Maiolino et al. 2004), suggesting that even at this epoch, significant amounts of dust are present near sites of active star formation. Alternatively, the unusual dust could be associated with the relatively nearby environment of the GRB only and not necessarily representative of the galaxy itself. However, the survival of this late dust limits the distance from the progenitor to at least 10–100 pc, suggesting that its association with the progenitor star-forming region cannot be too close.

The case of GRB 071025 is illustrative of the potential for early-time broad-band photometry of GRBs to reveal the chemical history of the early Universe (Hartmann et al. 2009). Well-characterized high-redshift bursts are unfortunately rare (5 yr into the *Swift* mission, only five other bursts to date have been confirmed to be at $z > 5$), and high-redshift events showing significant dust columns are even rarer (with the exception of the controversial 050904, above, none of the other $z > 5$ events show evidence for significant reddening; Ruiz-Velasco et al. 2007; Kann et al. 2007b; Tanvir et al. 2009; Greiner et al. 2009a). However, future GRB missions such as the Energetic X-ray Imaging Survey Telescope (EXIST; Grindlay et al. 2009) are likely to produce large advancement in our understanding of these events. While designed to search for GRBs at the redshift extremes ($z > 7$) and characterize these events spectroscopically, IR photometry and spectroscopy acquired of the much more frequent moderate-redshift events ($z = 4$–7) will place important constraints on the abundance and composition of dust during these early stages of cosmic evolution, when galaxies were in the active phase of assembly and the first generations of stars led to a rapid buildup of the metal content of the Universe.

[11] Unfortunately, the case of GRB 050904 is still ambiguous. Numerous other papers have investigated the dust properties of this event (Gou, Fox & Mészáros 2007; Kann et al. 2007a), and none of these other authors presented evidence favouring the Maiolino curve. Liang & Li (2009) have claimed detection of the 2175-Å feature. Therefore, we downloaded the available data on this source (Tagliaferri et al. 2005; Boër et al. 2006; Haislip et al. 2006; Kawai et al. 2006) and attempted to model the dust profile of this event using the same tools applied to GRB 071025, and found no evidence for a featured extinction curve. Indeed, the data are fully consistent with no extinction at all; our extinction fits converged to a simple power law with $\beta \sim 1.0$, in agreement with the comprehensive analyses of Kann et al. (2007a) and Gou et al. (2007).

[12] Although the extinction profile observed is an excellent match to the models of dust produced in SNe provided by Maiolino et al. (2004), we note that this does not demonstrate conclusively that this dust was formed in the SN explosion itself. Alternatively, the dust could be formed in the ISM (Draine 2009) from refractory elements produced in SNe, from early carbon stars (Sloan et al. 2009) or from an unknown pre-AGB formation mechanism.

ACKNOWLEDGMENTS

PAIRITEL is operated by the Smithsonian Astrophysical Observatory (SAO) and was made possible by a grant from the Harvard University Milton Fund, a camera loan from the University of Virginia, and continued support of the SAO and UC Berkeley. The PAIRITEL project is further supported by NASA/*Swift* Guest Investigator grants NNG06GH50G and NNX08AN84G. RAPTOR/Thinking Telescopes project is supported by the Laboratory Directed Research and Development (LDRD) programme at the LANL. JXP is supported by NASA/*Swift* Guest Investigator grants NNX08AN90G and NNX09AO99G. TK acknowledges support by the DFG cluster of excellence 'Origin and Structure of the Universe'. Part of the funding for GROND (both hardware and personnel) was generously granted from the Leibniz-Prize (DFG grant HA 1850/28-1) to Professor G. Hasinger (MPE).

We thank C. Melis at UCLA for acquiring the Lick IR photometry. We also thank D. A. Kann and the anonymous referee for useful comments and corrections on the manuscript. The W. M. Keck Observatory is operated as a scientific partnership among the California Institute of Technology, the University of California and the National Aeronautics and Space Administration (NASA). The Observatory was made possible by the generous financial support of the W. M. Keck Foundation. We wish to extend special thanks to those of Hawaiian ancestry on whose sacred mountain we are privileged to be guests. This research has made use of the NASA/IPAC Extragalactic Database (NED) which is operated by the Jet Propulsion Laboratory, California Institute of Technology, under contract with the National Aeronautics and Space Administration. We also acknowledge the hard work and efforts of the creators of other essential websites, in particular astrometry.net

REFERENCES

Abdo A. A. et al., 2009a, Sci, 323, 1688
Abdo A. A. et al., 2009b, ApJ, 706, L138
Akerlof C. et al., 1999, Nat, 398, 400
Barthelmy S. D., Butterworth P., Cline T. L., Gehrels N., Fishman G. J., Kouveliotou C., Meegan C. A., 1995, Ap&SS, 231, 235
Barthelmy S. D. et al., 2005, Space Sci. Rev., 120, 143
Bertin E., Mellier Y., Radovich M., Missonnier G., Didelon P., Morin B., 2002, in Bohlender D. A., Durand D., Handley T. H., eds, ASP Conf. Ser. Vol. 281, Astronomical Data Analysis Software and Systems XI. Astron. Soc. Pac., San Francisco, p. 228
Beuermann K. et al., 1999, A&A, 352, L26
Blake C. H. et al., 2005, Nat, 435, 181
Blake C. H., Bloom J. S., Latham D. W., Szentgyorgyi A. H., Skrutskie M. F., Falco E. E., Starr D. S., 2008, PASP, 120, 860
Bloom J. S., Starr D. L., Blake C. H., Skrutskie M. F., Falco E. E., 2006, in Gabriel C., Arviset C., Ponz D., Solano E., eds, ASP Conf. Ser. Vol. 351, Astronomical Data Analysis Software and Systems XV. Astron. Soc. Pac., San Francisco, p. 751
Bloom J. S. et al., 2009, ApJ, 691, 723
Boër M., Atteia J. L., Damerdji Y., Gendre B., Klotz A., Stratta G., 2006, ApJ, 638, L71
Burrows D. N. et al., 2005, Space Sci. Rev., 120, 165
Butler N. R., Kocevski D., 2007, ApJ, 663, 407
Butler N. R., Kocevski D., Bloom J. S., Curtis J. L., 2007, ApJ, 671, 656

Calzetti D., Armus L., Bohlin R. C., Kinney A. L., Koornneef J., Storchi-Bergmann T., 2000, ApJ, 533, 682
Chen S. L., Li A., Wei D. M., 2006, ApJ, 647, L13
Chincarini G. et al., 2007, ApJ, 671, 1903
Cohen M., Wheaton W. A., Megeath S. T., 2003, AJ, 126, 1090
Conconi P. et al., 2004, in Moorwood A. F. M., Masanori I., eds, Proc. SPIE Vol. 5492, Ground-Based Instrumentation for Astronomy. SPIE, Bellingham, p. 1602
Covino S. et al., 2004, in Moorwood A. F. M., Masanori I., eds, Proc. SPIE Vol. 5492, Ground-Based Instrumentation for Astronomy. SPIE, Bellingham, p. 1613
Draine B. T., 2009, preprint (arXiv:0903.1658)
Draine B. T., Hao L., 2002, ApJ, 569, 780
Dwek E., Galliano F., Jones A. P., 2007, ApJ, 662, 927
Elíasdóttir Á. et al., 2009, ApJ, 697, 1725
Fitzpatrick E. L., 1999, PASP, 111, 63
Fruchter A., Krolik J. H., Rhoads J. E., 2001, ApJ, 563, 597
Fynbo J. P. U. et al., 2009, ApJS, 185, 526
Gallerani S., Salvaterra R., Ferrara A., Choudhury T. R., 2008, MNRAS, 388, L84
Gehrels N. et al., 2004, ApJ, 611, 1005
Gou L.-J., Fox D. B., Mészáros P., 2007, ApJ, 668, 1083
Granot J., 2005, ApJ, 631, 1022
Granot J., Panaitescu A., Kumar P., Woosley S. E., 2002, ApJ, 570, L61
Greiner J. et al., 2008, PASP, 120, 405
Greiner J. et al., 2009a, ApJ, 693, 1610
Greiner J. et al., 2009b, ApJ, 693, 1912
Grindlay J., EXIST team, 2009, in Meegan C., Kouveliotou C., Gehrels N., eds, AIP Conf. Ser. Vol. 1133, Gamma-Ray Burst: Sixth Huntsville Symposium. Am. Inst. Phys., Melville, NY, p. 18
Guidorzi C. et al., 2009, A&A, 499, 439
Haislip J. B. et al., 2006, Nat, 440, 181
Hartmann D. H. et al., 2009, Astro2010: The Astronomy and Astrophysics Decadal Survey. Paper no. 115
Hillenbrand L. A., Foster J. B., Persson S. E., Matthews K., 2002, PASP, 114, 708
Kann D. A., Klose S., Zeh A., 2006, ApJ, 641, 993
Kann D. A., Masetti N., Klose S., 2007a, AJ, 133, 1187
Kann D. A. et al., 2007b, preprint (arXiv:0712.2186)
Kawai N. et al., 2006, Nat, 440, 184
Klotz A., Gendre B., Atteia J. L., Boër M., Coward D. M., Imerito A. C., 2009, ApJ, 697, L18
Kobayashi S., 2000, ApJ, 545, 807
Kobayashi Y. et al., 2003, in Oschmann, J. M., Stepp L. M., eds, Proc. SPIE Vol. 4837, Large Ground-Based Telescopes. SPIE, Bellingham, p. 954
Kocevski D., Butler N., Bloom J. S., 2007, ApJ, 667, 1024
Krühler T. et al., 2008, ApJ, 685, 376
Krühler T. et al., 2009a, ApJ, 697, 758
Krühler T. et al., 2009b, A&A, 508, 593
Kumar P., Granot J., 2003, ApJ, 591, 1075
Kumar P., Panaitescu A., 2000, ApJ, 541, L51
Kumar P., Panaitescu A., 2008, MNRAS, 391, L19
Küpcü Yoldaş A., Krühler T., Greiner J., Yoldaş A., Clemens C., Szokoly G., Primak N., Klose S., 2008, in Galassi M., Palmer D., Fenimore E., eds, AIP Conf. Ser. Vol. 1000, Gamma-Ray Bursts 2007. Am. Inst. Phys., Melville, NY, p. 227
Kurucz R. L., 1979, ApJS, 40, 1
Landolt A. U., 1992, AJ, 104, 340
Li Y., Li A., Wei D. M., 2008a, ApJ, 678, 1136
Li A., Liang S. L., Kann D. A., Wei D. M., Klose S., Wang Y. J., 2008b, ApJ, 685, 1046
Liang S. L., Li A., 2009, ApJ, 690, L56
McLean I. S. et al., 1993, in Fowler A. M., ed, Proc. SPIE Vol. 1946, Infrared Detectors and Instrumentation. SPIE, Bellingham, p. 513
McLean I. S. et al., 1994, in Crawford D. L., Craine E. R., eds, Proc. SPIE Vol. 2198, Instrumentation in Astronomy VIII. SPIE, Bellingham, p. 457
McQuinn M., Lidz A., Zaldarriaga M., Hernquist L., Dutta S., 2008, MNRAS, 388, 1101
Madau P., 1995, ApJ, 441, 18
Maiolino R., Schneider R., Oliva E., Bianchi S., Ferrara A., Mannucci F., Pedani M., Roca Sogorb M., 2004, Nat, 431, 533
Mészáros P., 2006, Rep. Progress Phys., 69, 2259
Molinari E. et al., 2007, A&A, 469, L13
Morgan H. L., Edmunds M. G., 2003, MNRAS, 343, 427
Nousek J. A. et al., 2006, ApJ, 642, 389
Oates S. R. et al., 2009, MNRAS, 395, 490
O'Brien P. T. et al., 2006, ApJ, 647, 1213
Oke J. B. et al., 1995, PASP, 107, 375
Pagani C., Racusin J. L., Kuin N. P. M., Holland S. T., Barthelmy S. D., Gehrels N., 2007, GCN Report 97.1
Page K. L. et al., 2007, ApJ, 663, 1125
Perley D. A. et al., 2008a, ApJ, 672, 449
Perley D. A. et al., 2008b, ApJ, 688, 470
Perna R., Lazzati D., 2002, ApJ, 580, 261
Perna R., Lazzati D., Fiore F., 2003, ApJ, 585, 775
Prochaska J. X. et al., 2009, ApJ, 691, L27
Racusin J. L. et al., 2008, Nat, 455, 183
Rees M. J., Meszaros P., 1992, MNRAS, 258, 41P
Rees M. J., Meszaros P., 1998, ApJ, 496, L1
Reichart D. E., 2001, ApJ, 553, 235
Roming P. W. A. et al., 2005, Space Sci. Rev., 120, 95
Ruiz-Velasco A. E. et al., 2007, ApJ, 669, 1
Rykoff E. S. et al., 2009, ApJ, 702, 489
Salvaterra R. et al., 2009, Nat, 461, 1258
Sari R., Piran T., 1999a, ApJ, 520, 641
Sari R., Piran T., 1999b, A&AS, 138, 537
Sari R., Piran T., Narayan R., 1998, ApJ, 497, L17
Savaglio S., Fall S. M., 2004, ApJ, 614, 293
Schady P. et al., 2007, MNRAS, 377, 273
Schlegel D. J., Finkbeiner D. P., Davis M., 1998, ApJ, 500, 525
Skrutskie M. F. et al., 2006, AJ, 131, 1163
Sloan G. C. et al., 2009, Sci, 323, 353
Stratta G., Perna R., Lazzati D., Fiore F., Antonelli L. A., Conciatore M. L., 2005, A&A, 441, 83
Stratta G., Maiolino R., Fiore F., D'Elia V., 2007, ApJ, 661, L9
Tagliaferri G. et al., 2005, A&A, 443, L1
Tanvir N. R. et al., 2009, Nat, 461, 1254
Tosti G. et al., 2004, in Moorwood A. F. M., Masanori I., eds, Proc. SPIE Vol. 5492, Ground-Based Instrumentation for Astronomy. SPIE, Bellingham, p. 689
Totani T., Kawai N., Kosugi G., Aoki K., Yamada T., Iye M., Ohta K., Hattori T., 2006, PASJ, 58, 485
Valiante R., Schneider R., Bianchi S., Andersen A. C., 2009, MNRAS, 397, 1661
Vestrand W. T. et al., 2002, in Kibrick R. I., ed., Proc. SPIE Vol. 4845, Advanced Global Communications Technologies for Astronomy II. SPIE, Bellingham, p. 126
Vestrand W. T. et al., 2005, Nat, 435, 178
Vestrand W. T. et al., 2006, Nat, 442, 172
Wainscoat R. J., Cowie L. L., 1992, AJ, 103, 332
Waxman E., Draine B. T., 2000, ApJ, 537, 796
Williams G. G. et al., 2004, in Fenimore E. E., Galassi M., eds, AIP Conf. Ser. Vol. 727, Gamma-Ray Bursts: 30 Years of Discovery. Am. Inst. Phys., Melville, NY, p. 723
Williams G. G., Milne P. A., Park H. S., Barthelmy S. D., Hartmann D. H., Updike A., Hurley K., 2008, in Galassi M., Palmer D., Fenimore E., eds, AIP Conf. Ser. Vol. 1000, Gamma-Ray Bursts 2007. Am. Inst. Phys., Melville, NY, p. 535
Woźniak P. R., Vestrand W. T., Panaitescu A. D., Wren J. A., Davis H. R., White R. R., 2009, ApJ, 691, 495
Yoshii Y., 2002, in Sato K., Shiromizu T., eds, New Trends in Theoretical and Observational Cosmology. Universal Academy Press, Tokyo, p. 235

Yoshii Y., Kobayashi Y., Minezaki T., 2003, American Astronomical Society Meeting Abstracts 202, 3803
Yost S. A. et al., 2007, ApJ, 657, 925
Zerbi R. M. et al., 2001, Astron. Nachr., 322, 275
Zhang B., Kobayashi S., Mészáros P., 2003, ApJ, 595, 950

SUPPORTING INFORMATION

Additional Supporting Information may be found in the online version of this article:

Table 3. Additional photometry of GRB 071025.

Please note: Wiley-Blackwell are not responsible for the content or functionality of any supporting materials supplied by the authors. Any queries (other than missing material) should be directed to the corresponding author for the article.

This paper has been typeset from a TEX/LATEX file prepared by the author.